

# Machine learning and parallelism in the reconstruction of LHCb and its upgrade

Marian Stahl on behalf of the LHCb collaboration

Physikalisches Institut der Universität Heidelberg, Germany

E-mail: [marian.stahl@cern.ch](mailto:marian.stahl@cern.ch)

**Abstract.** After a highly successful first data taking period at the LHC, the LHCb experiment developed a new trigger strategy with a real-time reconstruction, alignment and calibration for Run II. This strategy relies on offline-like track reconstruction in the high level trigger, making a separate offline event reconstruction unnecessary. To enable such reconstruction, and additionally keeping up with a higher event rate due to the accelerator upgrade, the time used by the track reconstruction had to be decreased. Timing improvements have in parts been achieved by utilizing parallel computing techniques that will be described in this document by considering two example applications. Despite decreasing computing time, the reconstruction quality in terms of reconstruction efficiency and fake rate could be improved at several places. Two applications of fast machine learning techniques are highlighted, refining track candidate selection at the early stages of the reconstruction.

## 1. Introduction

The LHCb experiment developed a new trigger strategy with a real-time reconstruction, alignment and calibration for the Run II data taking period (2015-2018). Hence, the trigger output is used to perform physics analyses without the need of an offline event reconstruction [1]. The main challenge has been to provide a faster and highly efficient reconstruction with a low rate of "fake" tracks, i.e. charged tracks that do not correspond to a real particle which passed through the detector. This challenge has been met by employing parallel computing techniques in timing critical, parallelizable stages, as well as machine learning in the early selection stages of the reconstruction algorithms. Further improvements and optimization of the reconstruction software will be essential for the LHCb upgrade for Run III data taking (scheduled 2021) where the experiment will move to a trigger-less readout system and a full software trigger [2-6].

This document is organized as follows: section 2 briefly describes the LHCb detector, the track reconstruction algorithms in place and plans for the upgrade track reconstruction. The use of parallelism in two timing critical parts of the reconstruction is discussed in section 3. Optimization of track candidate selection using machine learning is subject to section 4, where two applications will be reviewed.

## 2. The LHCb detector

The LHCb detector [7, 8], schematically shown in figure 1 is a single-arm forward spectrometer covering the pseudorapidity range  $2 < \eta < 5$ , designed for the study of particles containing  $b$  or  $c$  quarks. The detector includes a high-precision tracking system consisting of a silicon-strip vertex detector (VELO) surrounding the  $pp$  interaction region, a large-area silicon-strip detector (TT) located upstream of a dipole magnet with a bending power of about  $4\text{ Tm}$ , and three stations (T1-T3), consisting of silicon-strip detectors (IT) and straw drift tubes (OT) placed downstream of the magnet. The tracking system provides a measurement of momentum,  $p$ , of charged particles with a relative uncertainty that varies from  $0.5\%$  at low momentum to  $1.0\%$  at  $200\text{ GeV}$ . The minimum distance of a track to a primary vertex (PV), the impact parameter (IP), is measured with a resolution of  $(15 + 29/p_T)\mu\text{m}$ , where  $p_T$  is the component of the momentum transverse to the beam, in GeV.

Different types of charged hadrons are distinguished using information from two ring-imaging Cherenkov detectors (RICH1/2). Photons, electrons and hadrons are identified by a calorimeter system consisting of scintillating-pad (SPD) and preshower detectors (PS), an electromagnetic calorimeter (ECAL) and a hadronic calorimeter (HCAL). Muons are identified by a system composed of alternating layers of iron and multiwire proportional chambers (M1-M5).

The LHCb coordinate system is a right handed Cartesian system with the origin at the interaction point. The  $x$ -axis is oriented horizontally towards the outside of the LHC ring, the  $y$ -axis is pointing upwards with respect to the beam line and the  $z$ -axis is aligned with the beam direction.

The online event selection is performed by the trigger system, which is composed of three stages: a stage implemented in hardware known as Level 0 (L0) and two stages implemented in software called High- Level-Trigger (HLT1 and HLT2). The HLT1 performs a partial reconstruction of the candidates. In this stage most requirements are inclusive, which means that the selection is applied only to subset of the final state particles. A few exclusive algorithms are used to select specific decays at this trigger stage. The HLT2 contains hundreds of inclusive and exclusive algorithms which are more time-consuming and provide dedicated output for offline analyses.

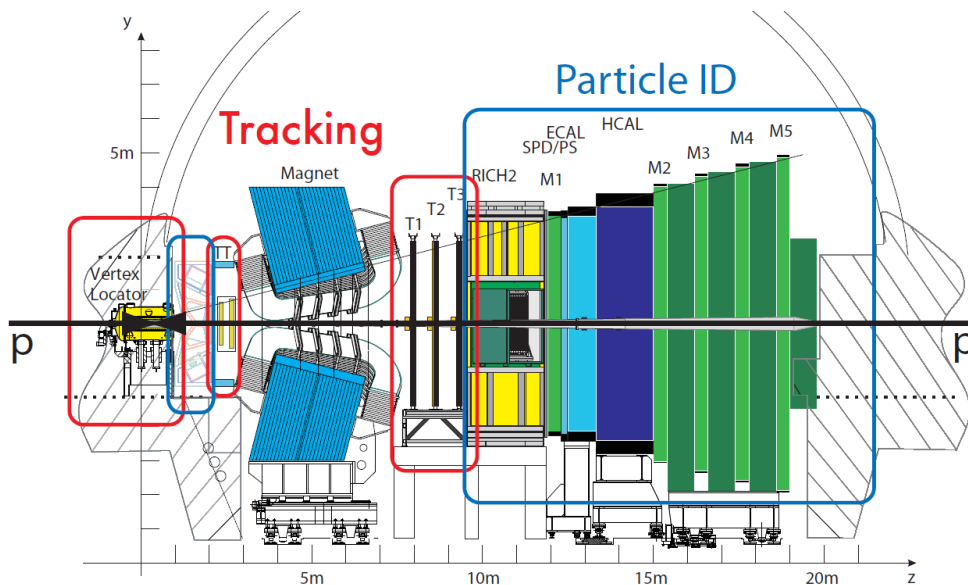


**Figure 1.** Schematic view of the LHCb detector at the LHC. The tracking subdetectors (VELO, TT, T stations) have been highlighted in red and the particle identification subdetectors (RICH1/2, calorimeters and muon system) in blue.

### 2.1. Track reconstruction

Figure 2 shows an overview of the different track types defined in the LHCb reconstruction: VELO tracks, which have hits in the VELO; upstream tracks, which have hits in the VELO and TT; T tracks, which have hits in the T stations; downstream tracks, which have hits in TT and the T stations; and long tracks, which have hits in the VELO and the T stations. The latter tracks can additionally have hits in TT.

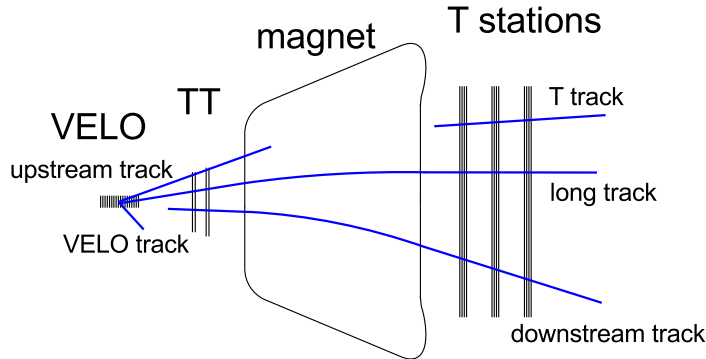


**Figure 2.** Track types in LHCb. Long tracks and downstream tracks are used for most physics analyses, the other types either serve as a component of another track type or are mainly used for detector studies.

Long tracks are the highest quality tracks comprising all available information from the trackers and are therefore used in most physics analyses. Downstream tracks mainly play a role in the reconstruction of daughters from long-lived particles which have decayed after the VELO (usually weakly decaying strange hadrons, such as  $\Lambda^0$  or  $K_S^0$ ).

Track reconstruction can be subdivided into a track finding/pattern recognition part and a track fitting part which is done by a Kalman filter. The basic track finding algorithms, called VELO tracking [9] and T seeding [10], reconstruct VELO and T track candidates which are used as seeds for upstream, long and downstream tracks. Long track candidates are found by two dedicated algorithms. The first, called forward tracking [11], starts with VELO or upstream tracks [12] and searches for corresponding hits in the T stations. The second, called track matching [13, 14], uses both VELO and T tracks as input and matches them in the magnet region. Downstream tracks use T tracks as seed and searches for corresponding clusters in the TT [15]. The outputs of all algorithms are merged, eliminating candidates that were found twice.

### 2.2. Reconstruction sequence in Run II and the upgrade

The Run II trigger, schematically shown on the left of figure 3, uses different track reconstruction sequences in the fast (HLT1) and full (HLT2) stage of the software trigger. In HLT1, all VELO tracks are reconstructed and fitted with a simplified Kalman filter, allowing for single rescattering at the sensor planes, and then used to find the primary vertices. VELO track trajectories are then extrapolated to the TT to reconstruct upstream tracks. In addition, the charge of the track can be estimated due to the magnetic fringe field in the TT. The upstream track candidates are then used as input to a fast version of the forward tracking algorithm, where only long track candidates with  $p_T > 500$  MeV are accepted. The found long track candidates are fitted with a Kalman filter.

The timing and fake rate of the HLT1 track reconstruction sequence in Run II profits from requiring a minimal transverse momentum, so that the forward tracking has to process only half

of the tracks [16]. Furthermore, by using the charge estimate of the upstream track candidate, the search window for potential hits only covers the region of the detector in which the particle will be deflected by the magnetic field as shown in the middle of figure 3. Another positive effect of using upstream tracks in the fast reconstruction sequence is that fake VELO tracks can be vetoed, since they are less likely to be confirmed with clusters in TT.

The HLT2 sequence of the forward tracking runs - with looser requirements - on VELO tracks that could not be promoted to long tracks in the HLT1 sequence. Details are discussed in section 4.2. In addition, standalone T tracks are matched with VELO tracks, to form long tracks, and with TT clusters, to form downstream tracks. All track candidates are fitted with a Kalman filter and clones from different algorithms are removed.

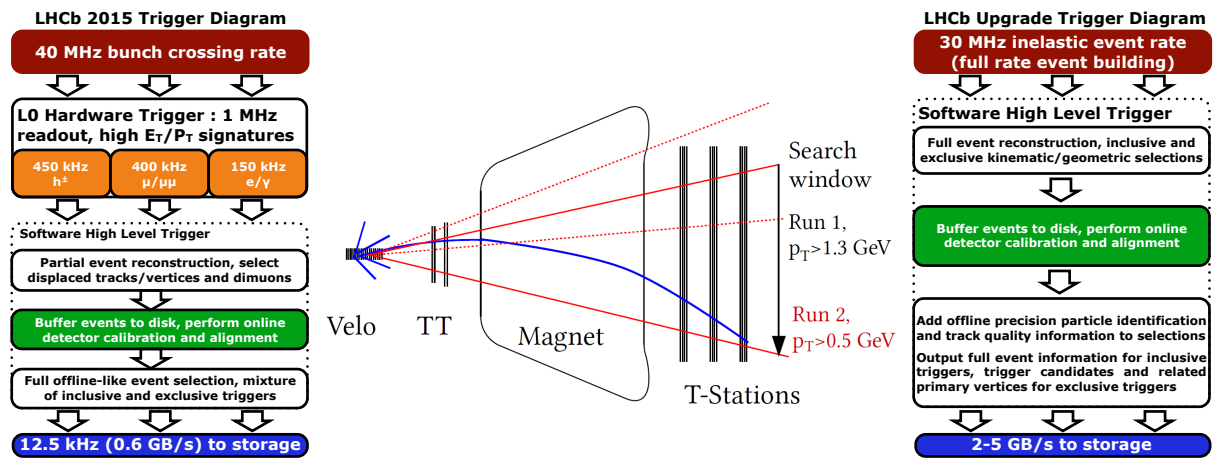


**Figure 3.** LHCb trigger scheme for Run II (left) and Run III (right). Long track reconstruction with the forward tracking algorithm in HLT1 comparing Run I and Run II (middle).

With the LHCb upgrade programme for Run III data taking, all three tracking detectors will be replaced. The current silicon strip VELO will be replaced by a pixel-based solution [3]; the TT by a silicon strip detector with higher granularity, called Upstream Tracker (UT); and the T stations by a Scintillating Fiber Tracker (SciFi), read out by silicon photomultipliers [5].

In Run III, the LHCb experiment will take data at an instantaneous luminosity of  $2 \cdot 10^{33} \text{ cm}^{-2} \text{ s}^{-1}$  - five times as high as in Run II. At this luminosity, the rate of potentially interesting physics would be too high to have a reasonable compromise of event reduction and efficiency with the simple selections of L0 hardware trigger. It was therefore decided to move to a trigger-less readout system and a full software trigger as shown on the right of figure 3. This puts strong constraints on the execution time of the tracking sequence in the fast trigger stage, which - at a higher occupancy - is expected to be reduced by a factor  $\sim 2.5$  compared to the current sequence. It will thus require massive use of cost-effective parallel computing techniques as well as finding an optimal working point in the trade-off between timing and track reconstruction efficiency at a low fake rate.

### 3. Parallelism

Although the reconstruction sequences became faster with the changes described in the previous section, further timing improvements were required. Data level parallelism in modern multi-core CPUs in the form of Single Instruction Multiple Data (SIMD) instructions are used to speed up time consuming parallelizable parts of the reconstruction code. These are purely mathematical computations requiring a significant amount of CPU cycles. However, most of the time consuming parts of the track finding algorithms are not parallelizable, since they are

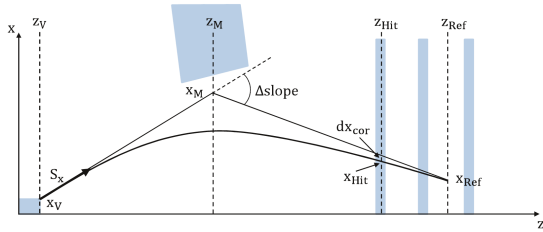


**Figure 4.** Sketch of seed track projection through the magnetic field. The true track trajectory is shown as curved line, whereas the simplified projection is given by straight lines intersecting in the middle of the magnet.

$$\begin{array}{ccc}
 F & C & F^T \\
 \begin{array}{|c|c|c|c|} \hline 1 & 2 & 3 & 4 \\ \hline 5 & 6 & 7 & 8 \\ \hline 9 & 10 & 11 & 12 \\ \hline 13 & 14 & 15 & 16 \\ \hline \end{array} & 
 \begin{array}{|c|c|c|c|} \hline 1 & 2 & 4 & 7 \\ \hline 2 & 3 & 5 & 8 \\ \hline 4 & 5 & 6 & 9 \\ \hline 7 & 8 & 9 & 10 \\ \hline \end{array} & 
 \begin{array}{|c|c|c|c|} \hline 1 & 5 & 9 & 13 \\ \hline 2 & 6 & 10 & 14 \\ \hline 3 & 7 & 11 & 15 \\ \hline 4 & 8 & 12 & 16 \\ \hline \end{array} \\
 \\ 
 \begin{array}{|c|} \hline 1 \\ \hline 2 \\ \hline 3 \\ \hline 4 \\ \hline \end{array} & = & 
 \begin{array}{|c|} \hline 1 \\ \hline 2 \\ \hline 4 \\ \hline 7 \\ \hline \end{array} * 1 + 
 \begin{array}{|c|} \hline 2 \\ \hline 3 \\ \hline 5 \\ \hline 8 \\ \hline \end{array} * 2 + 
 \begin{array}{|c|} \hline 4 \\ \hline 5 \\ \hline 6 \\ \hline 9 \\ \hline \end{array} * 3 + 
 \begin{array}{|c|} \hline 7 \\ \hline 8 \\ \hline 9 \\ \hline 10 \\ \hline \end{array} * 4
 \end{array}$$

**Figure 5.** Illustration of first parallelizable step of the transform  $F \cdot C \cdot F^T$ .

contained in bodies of conditional statements which are predicate to whether a computation is executed or not.

### 3.1. SIMD in forward tracking

Each of the tracking stations has four detection layers in an  $(x-u-v-x)$  arrangement with vertically oriented modules in the first and the last layer and rotated modules by a stereo angle of  $-5^\circ$  and  $+5^\circ$  in the second and the third layer, respectively. In the forward tracking algorithm, trajectories defined by a seed track (either VELO or upstream tracks) and a hit in the  $x$ -layers of the T stations, are projected through the magnetic field into a plane parallel to the tracking stations at a given  $z$  position ("Hough plane"). For an ideal magnet, the track trajectory outside the magnetic field could be described by two straight lines, whose extrapolations intersect in the middle of the magnet, as shown in figure 4. But magnetic fringe fields well outside the magnet volume, reaching at least up to the first T station, force the use of an empirically found cubical parametrization of the projection trajectory. This projection of seed tracks is done for every hit in the  $x$  layers of the tracking stations independently and is therefore an optimal use case for SIMD instructions. A timing improvement of 40% has been reached in this part of the code. This is close to the theoretical maximum of 50%, using `doubles` in the lowest common instruction set extension on the HLT computing farms - SSE2. Some percent in timing are lost by arranging the data into SIMD-usable form.

### 3.2. SIMD in track fitting

Track fitting is done with a Kalman filter to get the best track-parameter estimates. The fitting stage is the largest timing contributor in the HLT1 reconstruction sequence; mainly due to expensive calculus such as solving differential equations for the propagation through the magnetic field with the Runge-Kutta method or  $5 \times 5$  matrix operation needed by the Kalman filter. SIMD instructions are used for transportation of the covariance matrix from state  $k$  to state  $k + 1$ . This operation requires matrix multiplications of the form  $F \cdot C \cdot F^T$ , with a transport matrix  $F$  and a symmetric covariance matrix  $C$ . The first parallelizable step of multiplying  $C$  with the first column of  $F^T$  for  $4 \times 4$  matrices is shown in figure 5 and amounts to 16 multiplications and 3 additions. This reduces to 7 operations using the Advanced Vector Extensions (AVX) instruction set, which allows to process 4 `double` values in parallel. In the case of  $5 \times 5$  matrices, reordering the multiplications such that they are vectorized reduces the time consumption by about a factor of 2, while AVX would lead to a factor 5.

## 4. Machine learning

### 4.1. Fake track rejection

Fake long tracks can originate from falsely reconstructed track segments in the VELO or the T stations, from a mismatch of VELO and T station segments or from hadronic interaction of particles with the detector. During reconstruction, most of the fake long tracks originate from hadronic interactions, followed by fake track segments in the T stations and mismatched segments, while fake reconstruction of VELO segments occur at lower rate. Mismatched track segments are due to the long lever arm between the tracking stations up- and downstream of the magnet and remain to be the most abundant category after fake track rejection.

To discriminate between good and fake tracks, a fast artificial neural network classifier in form of TMVA's [17] MultiLayerPerceptron (MLP) is used in both stages of the software trigger after track fitting. While the "ghost probability" - the name of the MLP's response - was an offline quantity during Run I, a huge speed-up by a factor  $\sim 90$  allowed for its processing in HLT2 in 2015. A cut on the track  $\chi^2/\text{nDoF}$  of the track fit was used to reject ghost tracks in Run I and in HLT1 in 2015. Since 2016 the fake track rejection also runs in the HLT1 reconstruction sequence, leading to a significant speed-up of subsequent algorithms.

Main advances in mentioned speed-up come from choosing  $1/\sqrt{1+x^2}$ , rather than  $\tanh(x)$  as activation function, amounting to a factor 50 in terms of CPU-cycles; but also from choosing input variables which themselves are already available or do not require much additional computing time; and finally from manual optimization of the automatically generated class file for the TMVA reader [18]. Using AVX instructions, given the  $1/\sqrt{1+x^2}$  activation function, the number of CPU cycles could potentially be reduced by more than a factor of 2 in future applications.

The MLP uses 21 input variables and one hidden layer with 26 nodes. No performance gain from a deeper hidden layer structure, more layers, or human assisted learning was observed. To obtain a physical interpretation to the response, a probability integral transform - also referred to as "flattening" or "rarity transformation" - is obtained as a linear spline fit to the cumulative network response for fake tracks in simulated events. The performance of the artificial neural network is illustrated in figure 6.

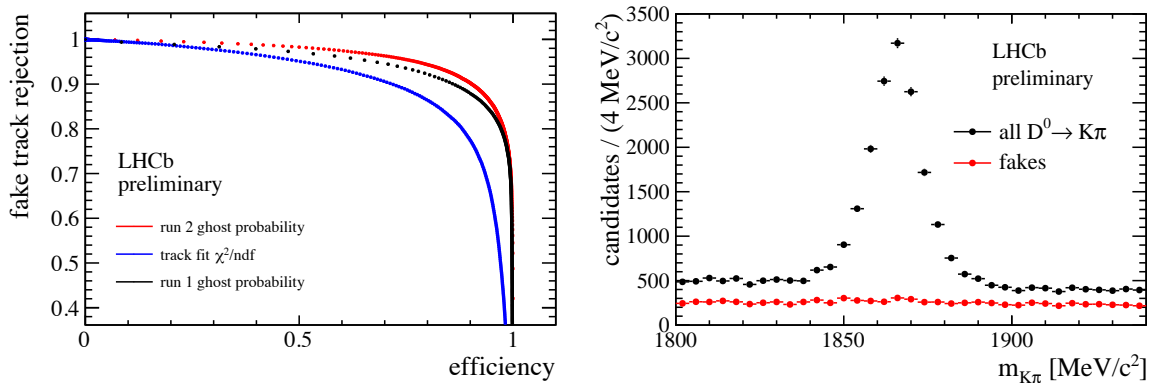


**Figure 6.** ROC curves for long tracks for the Run II ghost probability, the track  $\chi^2/\text{nDoF}$  and the Run I ghost probability obtained on a Run II dataset (left). At the optimal working point the fake track rate could be reduced from 22% to 14%, when comparing a cut on the track  $\chi^2/\text{nDoF}$  and the ghost probability.

$D^0 \rightarrow K\pi$  candidates from HLT2 output without cut on the ghost probability and events rejected by a cut on the ghost probability of 30% (right).

#### 4.2. Machine learning in the forward tracking

The forward tracking algorithm has undergone a major revision for 2016 data taking. Apart from re-tuning its parameters to adapt to Run II conditions, two artificial neural networks have been implemented to increase reconstruction efficiency and reject fake track candidates in the early stages of the reconstruction.

The forward tracking uses upstream tracks as seed tracks in HLT1 and VELO tracks as seeds in HLT2. A search window in the T stations is computed based on the seed track information. All T station hits in the  $x$ -layers are projected into a reference plane where - in form of a cluster search -  $x$ -track candidates are built. A  $\chi^2$  fit to these candidates is performed and hit-outliers are removed. After that, hits in the  $u$  and  $v$  modules are added and a similar  $\chi^2$  fit is performed, where outliers are removed. Track candidates that pass certain quality criteria are stored in a container which is an input to the Kalman filter. In HLT1,  $x$ -track candidates are only build if the corresponding cluster had at least one hit in 5 of 6 T station  $x$ -layers. In HLT2 the clustering runs with the same conditions, but if no long track candidate could be built from a seed track, a recovery loop (RL) is run where also  $x$ -track candidates are taken into account, which come from clusters with at least one hit in 4 T station  $x$ -layers.

One of the two neural networks is used to reject bad track candidates just before the track is stored for the Kalman filter. This network is evaluated in both reconstruction sequences of the trigger, using a slightly looser response cut in HLT2. The other network response is used to reject bad track candidates in the recovery loop of the HLT2 sequence for  $x$ -track candidates with only one hit in four different  $x$ -layers to reduce the large combinatorial background.

The artificial neural networks are again TMVA's MLPs which have been trained to optimize fake track rejection at a given efficiency of 99 or 97%. It was found that the classification performance improved with a deep hidden layer structure and larger number of parameters, even though some of them highly correlated. The MLP in the recovery loop has 9 input parameters and 2 hidden layers with 16 and 10 nodes, whereas the MLP for the final candidate selection has 16 input parameters and 3 hidden layers with 17, 9 and 5 nodes. The Rectified Linear Unit (ReLU) ( $\max(0, x)$ ) was chosen as activation function to ensure fast computation of the network response.

The performance of both neural networks was evaluated on Monte Carlo and validated with minimum bias data. Slight differences were found and the parameters of the forward tracking algorithm were adjusted accordingly. The performance results of the so found set of parameters is summarized in table 1. The neural networks contribute 0.5% and 2% to the execution time of the forward algorithm. Even though the forward tracking became slightly slower, the time consumption of the Kalman filter, and eventually the whole reconstruction sequence, was reduced due to the removal of fake tracks.

## 5. Conclusion

The LHCb experiment moved to a new trigger strategy with a real-time reconstruction, alignment and calibration for Run II data taking. To maximize the output of interesting events from the software trigger, the execution time of the track reconstruction sequences was decreased by an overall factor of two. This crucial speed-up was achieved with the help of SIMD instructions to increase the speed of the code and machine learning to efficiently remove fake tracks already in the early stages of the reconstruction. Ever faster algorithms exploiting parallelism and machine learning will be needed for Run III data taking, where LHCb will move to a trigger-less readout system and a full software trigger.

**Table 1.** Overview over the most important measures for the improved forward tracking. Timing and fake rates are given relative ( $= X_{new}/X_{ref} - 1$ ) to the previous (2015) forward tracking. The changes in efficiency are absolute changes.  $\varepsilon$  long and  $\varepsilon$  long from B (i.e. from a hadron containing a  $b$ - or  $\bar{b}$ -quark) were extracted after all reconstruction steps, while the HLT1 efficiency has to be evaluated at an intermediate step. The absolute reference fake rate at this stage of the reconstruction was 33% and 5.9% in HLT1. The absolute efficiencies given here are all  $\sim 90\%$ . Figures without recovery loop are given as optional setting.

MC performance 2016 w.r.t. 2015	$\nu = 1.6$	
	with RL	without RL
timing HLT1	$\pm 0.0\%$	
timing HLT2	+ 4.0 %	- 38.0 %
fake rate	- 26.9 %	- 35.1 %
fake rate HLT1	- 14.1 %	
$\varepsilon$ long	+ 0.5 %	+ 0.1 %
$\varepsilon$ long from B	+ 0.2 %	- 0.2 %
$\varepsilon_{\text{HLT1 long from B } p > 3, p_T > 0.5 \text{ GeV}}$	+ 0.1 %	

## References

- [1] Aaij R *et al.* 2016 *Comput. Phys. Commun.* **208** 35–42
- [2] Bediaga I *et al.* (LHCb collaboration) 2012 LHCb-TDR-012
- [3] Bediaga I *et al.* (LHCb collaboration) 2013 LHCb-TDR-013
- [4] Bediaga I *et al.* (LHCb collaboration) 2013 LHCb-TDR-014
- [5] Alves Jr A A *et al.* (LHCb collaboration) 2014 LHCb-TDR-015
- [6] Bediaga I *et al.* (LHCb collaboration) 2014 LHCb-TDR-016
- [7] Alves Jr A A *et al.* (LHCb collaboration) 2008 *JINST* **3** S08005
- [8] Aaij R *et al.* (LHCb collaboration) 2015 *Int. J. Mod. Phys.* **A30** 1530022
- [9] Callot O 2011 LHCb URL <https://cds.cern.ch/record/1322644>
- [10] Callot O and Schiller M 2008 URL <https://cds.cern.ch/record/1119095>
- [11] Callot O and Hansmann-Menzemer S 2007 URL <https://cds.cern.ch/record/1033584>
- [12] Bowen E E, Storaci B and Tresch M 2016 URL <https://cds.cern.ch/record/2105078>
- [13] Needham M and Van Tilburg J 2007 URL <https://cds.cern.ch/record/1020304>
- [14] Needham M 2007 URL <https://cds.cern.ch/record/1060807>
- [15] Callot O 2007 URL <https://cds.cern.ch/record/1025827>
- [16] Storaci B 2015 *J. Phys.: Conf. Ser.* **664** 072047. 6 p URL <http://cds.cern.ch/record/2017850>
- [17] Hoecker A, Speckmayer P, Stelzer J, Therhaag J, von Toerne E and Voss H 2007 *PoS ACAT* 040
- [18] Seyfert P <https://github.com/pseyfert/tmva-mlp>